Comb-locked deep-ultraviolet laser system for precision mercury spectroscopy

Comb-locked deep-ultraviolet laser system for precision mercury spectroscopy

Stefania Gravina, Naveed A. Chishti, Antonio Castrillo, and Livio Gianfrani*
Department of Mathematics and Physics, Università degli Studi della Campania "Luigi Vanvitelli"

Alessia Sorgi and Pablo Cancio Pastor
National Institute of Optics (INO) - National Research Council (CNR), Firenze

Cecilia Clivati, Fabio Bertiglia, Giuseppina Lopardo, and Filippo Levi
National Institute of Metrological Research (INRiM), Torino

Gianluca Galzerano
Institute for Photonics and Nanotechnologies (IFN) - National Research Council (CNR), Milano

Doppler-broadening gas thermometry is extended to the deep-ultraviolet domain using a comb- locked laser frequency chain, expressly developed for precision spectroscopy of mercury vapors at the wavelength of 253.7 nm, in coincidence with the $(6s^2)$ $^1S_0 \rightarrow (6s6p)$ $^3P_1$ intercombination line. The system is based on a double-stage second-harmonic generation process of an external-cavity diode laser at 1014.8 nm, which is frequency locked to a self-referenced optical frequency comb synthesizer by means of an efficient nonlinear frequency-mixing scheme. An absolute frequency axis in the UV region is produced by scanning the comb repetition rate, with the entire frequency
chain following the reference comb tooth. The complete characterization of the phase noise of the comb-locked near-infrared laser demonstrates line-emission narrowing down to the limit imposed by the coherence of the comb teeth. After a proper processing of the phase noise, the Gaussian and Lorentzian components of the width of the UV radiation are determined. This is useful to estimate the instrumental perturbation to the probed mercury line for the aims of thermodynamic temperature metrology. In this regard, the preliminary spectroscopic results are quite promising, despite the difficulties arising from the short wavelength of operation.

I. INTRODUCTION

Doppler broadening thermometry (DBT) is a very powerful method that allows one to probe directly the thermal motion of the particles of a gas at the thermo- dynamic equilibrium [1]. It is based on the high-fidelity recording of the shape of an atomic or molecular transition to retrieve the Doppler width, from which the thermodynamic temperature can be determined by using the Boltzmann constant k_B, whose value is fixed in the new International System of Units, since 20 May 2019. So far, this method has been implemented in the near- and mid- infrared spectral regions, mostly using molecular targets. The present article reports on the first extension of DBT to the deep-ultraviolet domain, in a dilute atomic gas, with the obvious advantage of benefiting from a larger Doppler-broadening effect. This is done by using a probe laser in the deep-ultraviolet spectral region, traceable to the primary frequency standard using a self-referenced fiber comb in the near-infrared.

Optical frequency combs in the visible/near-infrared regions represent an indispensable tool for optical metrology and fundamental physics. Thanks to the architecture of phase stabilized mode-locked oscillators, they provide a bridge between optical and microwave domains and enable highly precise absolute measurements of optical frequencies [2]. Such an extraordinary feature has revolutionized the field of precision laser spectroscopy, in the last two decades, thus producing a significant impact in our understanding of fundamental questions in nature, including the search for tiny variations of fundamental physics constants [3, 4] as well as validity tests of quantum electrodynamics (QED) [5] or the search for the solution of the proton size puzzle [6]. It is well known that comb technologies are employed as transfer oscillators to compare different species of optical atomic clocks, potentially facilitating a definition of the second with unprecedented accuracy [7]. Nowadays, the remarkable precision of optical frequency combs can be extended to exotic spectral regions, such as the deep-, extreme- and vacuum- ultraviolet ranges, by using cavity-enhanced high-order harmonic generation [8], thus following the pioneering work of T.W. Hänsch and co-workers [9].

For the aims of this work, we developed a frequency chain that reaches the UV region around 253.7 nm starting from the wavelength of 1014.8 nm, as provided by an external-cavity diode laser (ECDL, hereafter referred to as the pump laser, PL), this latter being locked to a near-infrared optical frequency comb synthesizer. For the application to temperature metrology, it is necessary to investigate the spectral purity of the UV radiation.

To this purpose, the PL frequency is compared with an ultra-narrow linewidth cw laser source emitting at 1542 nm. The frequency difference between such laser and PL is bridged by the optical frequency comb, following the method of the direct optical digital synthesis (DODS) [10, 11]. By using this technique, in conjunction to a phase-noise analyzer, phase fluctuations between the two lasers can be detected without any contribution of the comb phase noise. The linewidth of the pump laser is determined from the measured frequency-noise power spectral density by

means of the so-called β-line approach [12, 13]. Furthermore, the general method based upon the autocorrelation function of the light field enabled us to reconstruct the emission profile at 253.7 nm [14, 15].

Comb-assisted spectroscopic measurements on mercury vapors are reported. More particularly, we describe the refined measurement of the shape of the mercury intercombination line at 253.7 nm in the linear regime of radiation-matter interaction. This line has been the subject of extensive investigations, very recently [16, 17]. The simultaneous retrieval of the line center frequency and Doppler width demonstrates the possibility of doing primary determinations of the thermodynamic temperature of a low-pressure vapor sample, adopting a Voigt convolution as a lineshape model. In fact, the use of a di- lute atomic sample leads to a significant simplification of lineshape modeling and fitting, since collisional narrowing effects are completely avoided, differently from what has been observed with molecular samples [18–20]. The main advantages of probing a mercury line in the deep- UV are discussed in comparison to alkali-metal vapors, such as rubidium and cesium, whose D1 and D2 lines were tested for Doppler-broadening experiments in the near-infrared [21–24].

II. THE UV ABSORPTION SPECTROMETER

The experimental setup is depicted in Fig. 1. The laser source is based on the double-stage duplication of the ECDL at 1014.8 nm, as already described elsewhere [25]. Very briefly, the first stage of second harmonic generation occurs in a fiber-coupled periodically poled lithium niobate (PPLN) crystal waveguide, pumped by the ECDL. A high power diode laser at 507.4 nm, which is injection locked to the generated green radiation, is duplicated in a 12-mm long beta-barium borate (BBO) crystal inside a bow-tie cavity, thus producing the coherent UV radiation at 253.7 nm. The cavity is locked to the incoming beam through the H¨ansch-Couillaud technique [26]. The produced UV power goes up to 250 µW on a single mode in the continuous wave regime. In order to further improve the spatial beam quality profile, which is affected by the BBO crystal walk-off, the radiation is focused with a f = 50 mm lens into a 50 µm pinhole placed at the beam waist and aligned using a three-axis stage. About 20% of optical power is still available in the transmitted TM00 mode, which is enough for our application. The UV radiation passes through an acousto-optic modulator (AOM, Brimrose #2108-AO-20947), which is used to stabilize the UV power. To this purpose, a portion of the first-order diffracted UV beam is monitored by a silicon carbide (SiC) photodetector whose output signal is sent to a proportional-integrator circuit to actively control the RF power driving the AOM. The relative power stability is better than 10−4 over a time span of about 20 minutes. The remaining portion of the UV beam (whose power amounts to about 5 µW) is sent to a temperature- stabilized cell containing the mercury vapors. Manufactured by Precision Glassblowing Inc., the cell consists in a 2-cm long quartz tube sealed at the two ends by a pair of wedged windows with a diameter of 25.4 mm. A cylindrical reservoir is welded in the middle of the cell, in the transverse direction as compared to the cell's axis. As guaranteed by the manufacturer, the reservoir is filled with liquid mercury and the cell is closed in a ultra-high vacuum environment, so that ultra-pure Hg vapors are in equilibrium with the liquid phase. The cell is placed in a thermostatic vacuum chamber, whose details can be found in Ref. [27]. As a result, the temperature is actively controlled and maintained stable within 0.05 mK at the triple point of water for several hours. A sub-mK stability was achieved at other temperatures in a relatively wide range between -50 ◦C up to +50 ◦C. The cell's temperature is provided by a capsule-type standard platinum resistance thermometer (c-SPRT, Hart Scientific, model 5686), connected to a precision resistance bridge (Automatic Systems Laboratories, model F18). The bridge reads the resistance ratio between the thermometer and a temperature-stabilized standard resistor. The c-SPRT was calibrated at INRiM, the Italian National Metrological Research Institute, in accordance to the International Temperature Scale (ITS-90) in the sub-range between the temperatures of the triple point of mercury (-38.83 ◦C) and the gallium melting point (29.76 ◦C). Furthermore, the chamber is magnetically shielded by a mu-metal layer, in order to prevent the interaction of the Hg atoms with the Earth magnetic field.

After the interaction with mercury vapors, the transmitted UV beam is focused on a second SiC photodetector, whose output signal is measured by means of a 6½-digit multimeter with a gate time of 3 ms, this latter giving the observation time for each point of the absorption spectrum.

The pump ECDL is referenced to an optical frequency comb synthesizer (OFCS, from Menlo Systems, model FC-1500-250-WG), based on an erbium-doped mode- locked femtosecond fiber laser at 1560 nm, with a repetition rate of 250 MHz. The comb repetition rate (frep) and the carrier-envelope offset frequency (fceo) are stabilized against a GPS-disciplined rubidium clock, whose 1-s relative stability amounts to about 2.5×10−12. Therefore, any comb tooth of the supercontinuum between 1050 and 2100 nm represents an absolute frequency reference given by $f_n = n \times f_{rep} + f_{ceo}$, n being the tooth order.

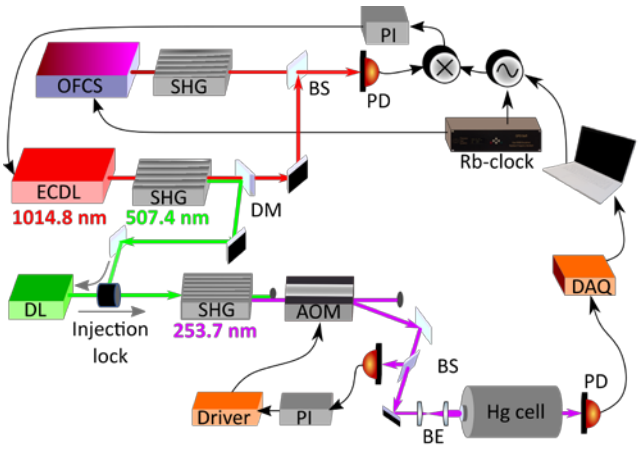

FIG. 1. Schematic of the UV spectrometer that highlights the comb-locked UV source, the isothermal cell containing the Hg vapors, and the acquisition electronics. DL stands for diode laser; SHG, second harmonic generation stage; BS, beam splitter; DM, dichroic mirror; BE, beam expander; PD, photodiode, PI, proportional-integrative servo circuit; DAQ, data acquisition board.

Due to the sharp cut-off of the supercontinuum spectrum at 1050 nm, beating between the comb and the pump ECDL required the implementation of a new scheme. To this aim, the longer wavelength portion of the comb (above 2 μm) is frequency-doubled through a single pass in a 3-mm-long MgO-doped periodically poled lithium niobate crystal (Covesion Ltd, MSHG2100-0.5- 3), to produce comb radiation centered at 1020 nm with a width of about 20 nm and a peak power of about 1.5 μW at the resolution bandwidth of 1 nm, as shown in Figure 2. Reflection losses in the SHG process are minimised by an antireflection (AR)-coating covering the bands from 1968 to 2270 nm and from 984 to 1135 nm, in the input and output facets of the crystal, respectively. The measured power at 1015 nm is about 600 pW per tooth.

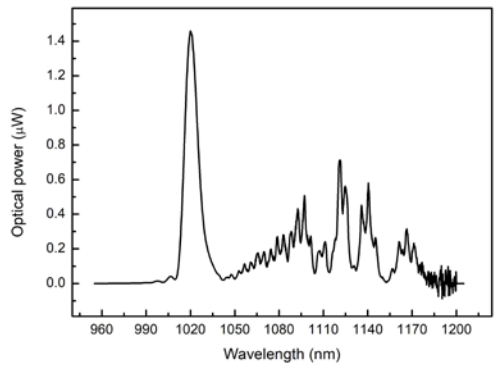

FIG. 2. The spectrum of the comb light after frequency duplication of the portion at wavelengths above 2 μm, as measured by means of an optical spectrum analyzer with a resolution bandwidth of 1 nm.

The frequency-doubled comb light is overlapped with the PL beam, spectrally filtered by a grating–lens–slit assembly, and sent to a fast photodiode to produce a beat note signal, which is effectively used for frequency locking the PL to the nearest tooth of the frequency-doubled comb, with an offset of 20 MHz. To this purpose, the error signal generated by a phase detector is processed by a proportional-integral-derivative (PID) controller and sent to the PL current driver. The beat note signals under weak- (black dots) and fast-lock (red dots) conditions are reported in Figure 3. The former configuration corresponds to a 100-Hz lock bandwidth (LBW) and low proportional gain so that the laser could be considered to operate under the free-running regime, while the latter corresponds to 10-kHz LBW and high proportional gain. The benefit of the PL locking to the comb in the reduction of the laser emission width is evident. A quantitative investigation of the coherence properties of the pump laser, which in turn determines the frequency stability of the UV radiation, required a thorough study of the beat note linewidths and of the phase noise, as reported in the Section that follows.

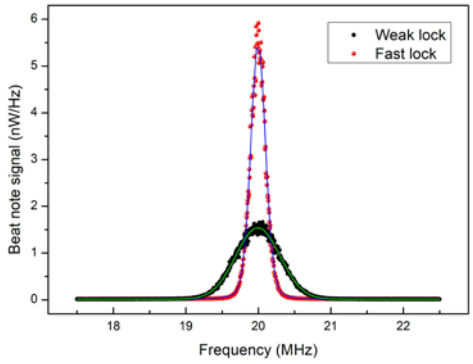

FIG. 3. Beat note measurements between the pump laser and the nearest tooth of the frequency-doubled comb at 1015 nm, with the ECDL in weak-lock (black dots) and fast-lock (red dots) conditions. The resolution bandwidth of the spectrum analyzer is set to 200 Hz (equivalent to an integration time of 5 ms). The signal-to-noise ratio amounts to about 30 dB, for the fast lock regime.

It is worth noting that, once the beat-note frequency, f_{beat}, of the PL with the comb is measured by means of a frequency counter, the absolute UV frequency, f_{UV}, can be determined from the following equation:

$$f_{UV} = 4 \times (m \times f_{rep} \pm f_{beat} \pm 2 \times f_{ceo}) - f_{AOM}, \quad (1)$$

m and f_{AOM} being the mode order at 1015 nm and the frequency of the RF signal driving the AOM, respectively. As it is well known, the ambiguity on the signs can be easily removed by slightly varying f_{ceo} and f_{rep} and observing the consequent variation of f_{beat}. The tooth order is unambiguously assessed by measuring the PL wavelength in the near-IR by means of a 9-digit wavemeter (Bristol Instruments, model 671A).

Under the fast-lock regime of operation, highly accurate scans of the PL frequency were performed by finely tuning the comb repetition rate. Doing so, continuous scans in the UV region as large as 4 GHz are achieved, with the frequency chain perfectly following the comb- traceable PL absolute frequency. To this purpose, a key ingredient revealed to be a feed-forward correction to the external cavity of the pump laser to avoid mode hops, as well as a similar one acting on the current of the green diode laser. This latter was necessary in order to maintain the injection from the seed light throughout the full frequency scan.

It is worth noting that the UV frequency is directly GPS-traceable to the primary standard with a precision and accuracy given by the OFCS frequency stability.

III. CHARACTERIZATION OF THE SPECTRAL COHERENCE OF THE NEAR-IR RADIATION

A first estimate of the ECDL linewidth was performed by fitting the PL-comb beat notes to Gaussian/Voigt spectral profiles. The beat note lineshape of the weak lock condition in Figure 3 is well reproduced by a Gaussian profile with a full-width at half-maximum (FWHM) of 716±7 kHz. This value can be mostly ascribed to the free-running linewidth of the ECDL since the comb-lock compensates for frequency drifts and jitters up to 100 Hz. Instead, under the fast lock condition, a Voigt fit of the beat note profile yields a width of about 240 kHz, namely, a factor of ~3 narrower, with a Gaussian component of 219±2 kHz and a Lorentzian one of 37±3 kHz. Presumably, these contributions are close to the lower limit that is imposed by the tooth linewidth of the SHG comb around 1015 nm. It is worth noting that the use of a Voigt convolution is justified by the fact that the emission spectrum of a single-mode semiconductor diode laser is typically given by a Voigt profile, which is the convolution of the Lorentzian spectrum associated with the white frequency noise and the Gaussian spectrum arising from the flicker noise [28].

In general, extrapolating the linewidth of a tested laser from the beat note with a reference laser is not an easy task, unless the tested laser has a much larger linewidth than the other. It is well known that the beat note can be even narrower than each laser if the phase noise of the two lasers is partially correlated, as in the case of the present work. For this reason, it is useful to quantify the comb tooth linewidth. To this aim, we observed and analyzed the beat note between a 100-Hz linewidth diode laser (from OEwaves, model OE4030, hereinafter referred to as the reference laser, RL) emitting at 1542 nm and the nearest comb tooth at this wavelength. The high spectral purity of such a laser is assured by the self- injection locking of the semiconductor diode to a high- quality factor whispering gallery mode of a crystalline optical resonator. A fraction of the comb, wavelength- division-multiplexing (WDM) filtered around 1542 nm, is mixed with the RL radiation by using a 90:10 fiber splitter, and sent to a fast InSb

photodetector. The detected beat note signal of Figure 4 is recorded on the spectrum analyzer with the same resolution bandwidth as the one shown in Figure 3. The nonlinear least-squares fit with a Voigt function, represented by the red line of Figure 4, gives a total FWHM of ~ 110 kHz, with a Gaussian contribution of 105±4 kHz and a Lorentzian one of 9±6 kHz. This measurement essentially gives the width of the comb teeth at 1542 nm, the RL linewidth being completely negligible. Considering that the SHG comb tooth linewidth is approximately a factor of 2 wider as compared to those above 2 μm wavelength and assuming that the comb coherence is maintained at all frequencies of the comb operation range, we can estimate a width (FWHM) of about 220 kHz for the generic tooth nearby 1015 nm. For fiber-based combs in the near-IR a gradual increase in phase noise was measured as one moves away in frequency from the carrier of the 1560 nm femtosecond laser [29]. Consequently, a larger linewidth could be expected for the comb teeth around 2030 nm with respect to those at 1542 nm. From these considerations, we can deduce that the pump laser is essentially narrowed down to the limit of the comb tooth at 1015 nm, but we cannot go much further than this qualitative information.

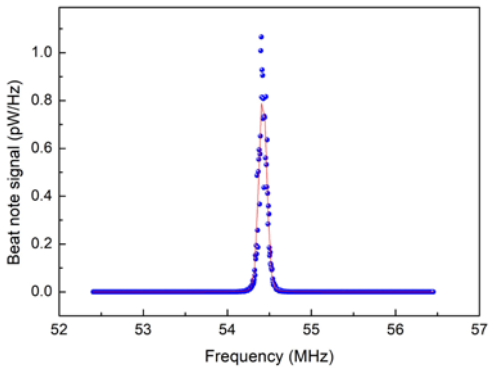

FIG. 4. Beat note measurement between the reference laser and the nearest tooth of the comb at 1542 nm. The heterodyne signal is recorded by means of a spectrum analyzer with a resolution bandwidth of 200 Hz. The red line represents the Voigt profile, as obtained from a nonlinear least-squares fit of the data.

A more quantitative investigation of the coherence properties of the PL was performed through the measurement of the phase noise of the beat note between the PL and RL sources. More particularly, we measured the phase noise of the comb-locked pump laser with respect to the ultra-narrow linewidth laser. The comparison between the spectral purity of the pump ECDL and the reference laser is possible by using the OFCS as a bridge between the two different wavelength values in the well- tested method of direct optical digital synthesis [10, 11].

Let's start with the beat of the PL with the frequency-doubled comb. The beat note frequency is given by:

$$f_{beat} = f_{PL} - (n_{PL} \times f_{rep} + 2 \times f_{ceo}), \qquad (2)$$

while the RL-comb beat note, f'_{beat}, results to be

$$f'_{beat} = f_{RL} - (n_{RL} \times f_{rep} + f_{ceo}). \qquad (3)$$

The fbeat and fbeat frequencies are centered at 20 MHz and ~54 MHz, respectively, as shown in Figures 3 and 4.
The first DODS step is to remove the fceo contributions to fbeat and fbeat. To this aim, the fbeat signal is conveniently RF-filtered and amplified. Similarly, the fceo beat signal is filtered, amplified and then power-splitted in two equal fractions. One of these fractions is RF frequency doubled and mixed to the fbeat signal and the other one is RF-mixed to the fbeat, thus resulting in a pair of fceo-free RF signals. Hence, the fbeat+fceo signal is direct-digital-synthesized by multiplying it by the 32-digit precise-factor nPL/nRL, resulting in a further RF-signal, which is RF-mixed with fbeat + 2 × fceo. So doing, we obtain a signal at the frequency fbeat given by:

$$f''_{beat} = f_{RL} \times \frac{n_{PL}}{n_{RL}} - f_{PL}, \qquad (4)$$

which allows us to compare the phase noise of the PL and RL sources without any contribution of the OFCS phase noise, which indeed cancels out. A simplified scheme of the employed RF-electronics is shown in Figure 5.

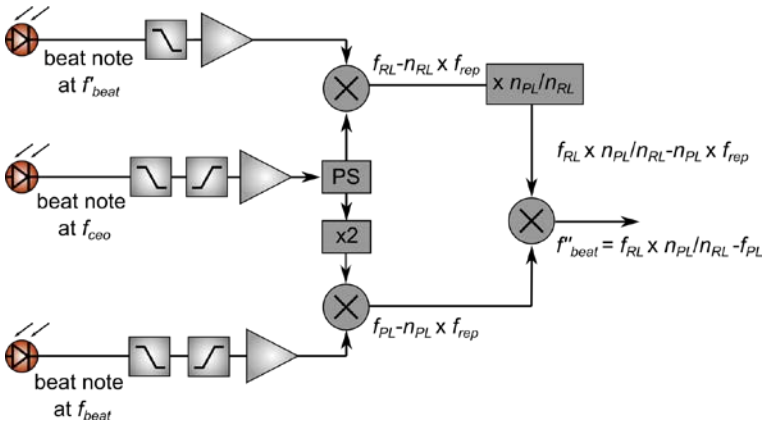

FIG. 5. Schematic representation of the electronic system used to perform the direct optical digital synthesis. PS, power splitter.

The phase noise power spectral density (PSD, expressed in rad2/Hz) of the fbeat signal is recorded by means of a high-sensitivity phase noise spectrum analyzer (Rohde & Schwarz, FSWP8) for Fourier frequencies between 1 Hz and 1 MHz. Typical acquisitions are shown in Figure 6. The upper (red) line corresponds to the phase noise PSD when the pump laser is weakly locked to the comb, basically the PL free-running condition. Similar acquisitions are done in the tight and fast lock configurations (see the blue and green lines, respectively, in the middle and at the bottom of Figure 6), with increasing cut-off frequencies of the integration stage of the PID electronics. Servo loop peaks are observed nearby the Fourier frequencies of 100 Hz, 300 Hz and 10 kHz as signatures of the loop-bandwidth for the weak, tight and fast lock conditions, respectively.

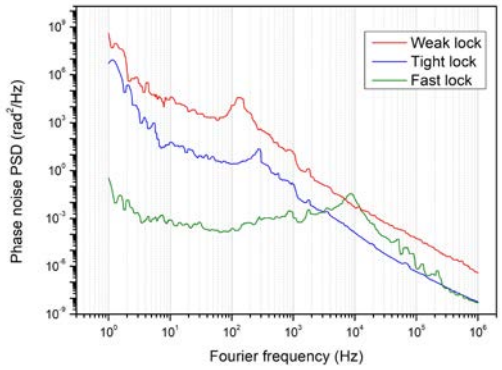

FIG. 6. Phase noise power spectral density of the beat note at f'_{beat} in different comb-locked configurations.

The laser excess noise in the low-frequency region (<1 kHz) is significantly reduced in the fast lock condition if compared with the other two configurations, with a phase noise suppression of several orders of magnitude. Consequently, also due to the negligible phase-noise contribution of the RL, we can hypothesize that, whereas only frequency drifts and very slow jitters are controlled for the weak and tight locks, narrowing of the PL linewidth to the SHG comb width can be expected only for the fast lock condition. The phase noise PSD can be converted into a frequency noise PSD, in Hz2/Hz, to extract quantitative information about the frequency noise and the emission linewidth of the pump laser. In fact, from the frequency noise PSD of Figure 7, the laser width can be retrieved after integration over a frequency range that is determined by the β-separation line [12, 13]. This latter is defined by the following equation:

$$\beta = 8\frac{\ln 2}{\pi^2} f, \qquad (5)$$

where f is the Fourier frequency.

The β-separation line displays geometrically the slow-modulation area of the PSD, Σ, affecting the laser lineshape. Specifically, this area is identified by the Fourier frequency interval for which the PSD values are greater than the β-separation line, shown as the red line in Figure 7. A laser width (FWHM), ΔL, of about 293 kHz is retrieved by using the following equation:

$$\Delta_L = \sqrt{8\Sigma \ln 2}. \qquad (6)$$

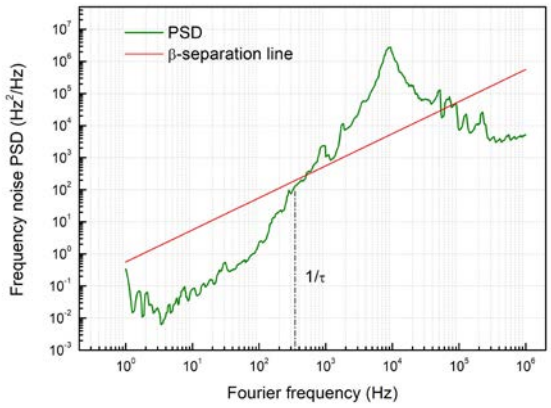

FIG. 7. Frequency-noise power spectral density of the detected beat note at fbeat while the pump laser is locked to the OFCS with 15-kHz integrator bandwidth. The β-separation line is also shown to display the region for which the PSD significantly contribute to the laser linewidth. The cut-off frequency is set to about 333 Hz corresponding to an observation time, τ , of 3 ms.

It is not surprising that the retrieved width is larger than the one of beat note in the fast lock regime, meaning that the PL phase noise is correlated to that of the comb tooth at Fourier frequencies smaller than 1 MHz. Therefore, it is confirmed that shrinking of the PL emission width close to the limit imposed by SHG comb coherence around 1015 nm was achieved. It is worth noting that the low-frequency noise region, below the limit imposed by the observation time (τ=3 ms), does not affect the laser emission profile.

IV. ESTIMATION OF THE SPECTRAL PROFILE OF THE UV RADIATION

In order to retrieve information about the profile of the UV radiation, we consider that frequency multiplication by a factor k leads to an increase of the phase noise power spectral density by a factor k2 [30]. Therefore, the phase noise of Figure 6, under the fast lock condition, is first multiplied by a factor of 16 and then converted into a frequency noise PSD. The UV emission spectrum is determined by using the exact method based on the autocorrelation function of the laser light field, E(t) [14]. In particular, this approach is based on the Wiener-Khintchine theorem, which relates the power spectrum W(ν) of the laser light and the autocorrelation function, Γ(t′) = ⟨E∗(t)E(t + t′)⟩, by the Fourier transform integral:

$$W(\nu) = 2\int_{-\infty}^{+\infty} e^{-i2\pi\nu t'}\Gamma(t')dt'. \qquad (7)$$

Considering a laser light field given by E(t) =E0ei[2πν0t+ϕ(t)], where ν0 is the oscillation frequency and ϕ(t) the phase noise, Equation 7 becomes as follows:

$$W(\nu) = 2\int_{-\infty}^{+\infty} e^{-i2\pi\nu t'} E_0^2 e^{i2\pi\nu_0 t'} \exp\left[-2\int_{1/\tau}^{\infty} S(f)\frac{sin^2(\pi f t')}{f^2}df\right]dt', \qquad (8)$$

S(f) being the frequency noise PSD in the UV region.

Equation 8 is numerically integrated from the cut-off frequency ($1/\tau$ = 333 Hz) to 1 MHz. The reconstructed spectrum is shown in Figure 8. The nonlinear least squares fit with a Voigt function gives a UV linewidth (FWHM) of about 1.35 MHz, with a Gaussian contribution, ΔL, of 1.3089±0.0008 MHz and a Lorentzian one, ΓL, of 69.6±1.2 kHz. These values could be intended as lower limit components to the UV linewidth. In fact, it is well known that the use of frequency doubling stages, such as the PPLN waveguide frequency doubler, can introduce some additional excess noise at low Fourier frequencies (<100 Hz), mostly ascribed to amplitude-tophase conversion that originates from changes of the differential refractive index of the SHG material, due to the induced temperature fluctuations [31, 32]. Consequently, it could be argued that an accurate determination of the UV line profile can only be recovered from phase noise measurements of the UV radiation. Nevertheless, our apparatus is expected to be poorly sensitive to low-frequency noise, because of the relatively small observation time (3 ms). For this reason, additional excess noise at low Fourier frequencies should not affect the UV radiation linewidth. The measured UV radiation linewidths shall be used as input parameters in the fitting procedure of Hg absorption spectra to retrieve the Doppler width and, consequently, the thermodynamic temperature, as it will be shown in the next section.

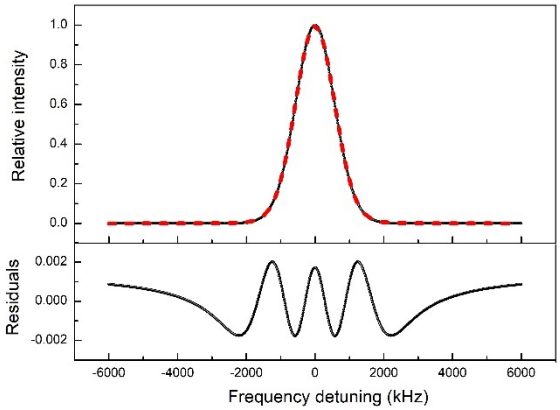

FIG. 8. Estimation of the UV emission profile in terms of relative intensity obtained by numerical integration of the Fourier transform of the laser light autocorrelation function using an observation time of 3 ms. The dashed (red) line represents the Voigt profile which best approximates the laser lineshape [12]. The fit residuals are shown in the lower panel.

V. COMB-CALIBRATED MERCURY SPECTROSCOPY

Mercury atoms were already considered an interesting choice for the aims of Doppler-broadening thermometry (DBT) by Truong et al. [24], although the wavelength of the intercombination transition was judged to be inconvenient. The preliminary results of this section show that a new mercury-based primary thermometer is a real possibility to be considered for the practical realization of the unit kelvin by means of an optical method. Table I shows a comparison between the ^{200}Hg $(6s^2)^1S_0 \rightarrow (6s6p)^3P_1$ line and the Rb and Cs lines for which successful DBT implementations have been carried out [21, 22]. The benefits of mercury seem obvious: a zero nuclear spin that means no hyperfine structure; a more favorable ratio of the Doppler to natural widths; a much larger absorption coefficient; a larger saturation intensity.

TABLE I. Main properties of the ^{200}Hg intercombination line compared with those of the ^{85}Rb D_2 and Cs D_1 lines. Columns from left to right show: atom; wavelength (λ); nuclear spin (I); ratio between Doppler (Δ_A) and natural (Γ_N) widths; absorption coefficient at 298 K (α_{RT}); ratio of hyperfine splitting (hfs) to Doppler width; saturation intensity (I_s).

Atom	λ (nm)	I	Δ_A/Γ_N	α_{RT} (cm^{-1})	hfs/Δ_A	I_s (mW/cm^2)
^{85}Rb D2 line	780	5/2	83	0.27	0,1	∼2
^{133}Cs D1 line	895	7/2	77	1.9	3.2	∼2.5
^{200}Hg	253	0	811	8.5	0	∼5

Figure 9 shows a typical absorption spectrum that results from a continuous scan of the UV frequency over a 3.5-GHz-wide

interval, in coincidence with the intercombination transition of the 200Hg isotope, at a temperature of 268.14997 (5) K. The absorption spectrum is obtained after averaging over 4 spectral acquisitions. It consists of 726 points, the frequency step being 4.73 MHz. The time span for each acquisition amounts to about 3 minutes. The residuals from a nonlinear least-squares fit to a Voigt convolution are also shown. More particularly, the spectrum is compared to the following function:

$$P(f_{UV}) = [P_0 + P_1 f_{UV}] \times e^{-A_{int} \times g(f_{UV} - f_0)}, \quad (9)$$

where P0 and P1 are two baseline parameters accounting for a residual linear variation of the incident power, f0 is the line center frequency, Aint is the frequency integrated absorbance, while g(fUV − f0) is the convolution of the normalized absorption lineshape function gA and the laser emission profile gL, as determined in Section IV.
More particularly, the double-Voigt convolution is given by:

$$g(f_{UV} - f_0) = \int_{-\infty}^{+\infty} g_L(f_{UV} - f') g_A(f' - f_0) df'. \quad (10)$$

It can be shown that the convolution of two Voigt functions is still a Voigt function, with Lorentzian and Gaussian components given by:

$$\Gamma = \Gamma_A + \Gamma_L$$

and

$$\Delta = \sqrt{\Delta_A^2 + \Delta_L^2},$$

where ΓA and ΔA are the homogeneous and Doppler width (FWHM) of the atomic transition, respectively. The theoretical profile, which is obtained by a least-squares optimization of the Doppler width, line center, line area, and baseline parameters, agrees well with the experimental lineshape, as evidenced by the flat residuals. In the fitting procedure, ΓA is set to the sum of the natural linewidth, namely, 1.272±0.008 MHz, as determined in [33], and the collisional width. In fact, despite the small Hg pressure, the collisional self-broadening effect may have a measurable influence. A first estimate of the Hg-Hg broadening coefficient can be found from the spectral analysis of ref. [33], which leads to 19±17 MHz/Pa. Its large uncertainty is due to the difficulties of retrieving small homogeneous widths (of the order of a few MHz) from broad Doppler-limited absorption spectra (whose width is at the GHz level). A more precise determination of the pressure broadening coefficient, coming from Lamb-dip spectra as a function of Hg vapor pressures (ranging from 0.09 to 0.2 Pa), gives 11±2 MHz/Pa. This relatively large value tells us that the collisional broadening effect cannot be neglected, differently from what initially estimated [34]. Lamb dip spectroscopy of the Hg intercombination line will be the subject of a future work. For the aims of the present paper, we use this latter determination. Hence, the collisional width was set to 180 kHz with an uncertainty of 30 kHz. Furthermore, ΓL and ΔL were fixed at the measured values. It should be noted that optical pumping perturbations to the absorption profile are negligible, the intensity of the UV radiation being about 4 orders of magnitude smaller than the saturation intensity of the 1S0 →3P1 transition.
Twenty repeated spectral acquisitions were performed, under the same experimental conditions. After spectral averaging and fitting, a total of five Doppler width determinations were obtained, along with the absolute center frequencies. The mean value of the Doppler width results to be 0.97999±0.00038 GHz, while the absolute center frequency is 1181550971726±130 kHz. These numbers translate into a thermodynamic temperature of 268.16±0.21 K, the reported uncertainty being of pure statistical nature at 1σ confidence level. The spectroscopic value is in good agreement with the set point. It is worth noting that the Gaussian component of the UV radiation width has a small influence on the temperature retrieval, the perturbation being at the part-per-million (ppm) level. A larger influence arises from ΓL. In fact, if ΓL is set to 0 kHz, the spectroscopic temperature is increased of 20 mK, namely, ∼75 ppm in relative terms. The uncertainty budget is largely dominated by the statistical component (also known as type A component), the second largest entry being associated to the collisional width. Indeed, its uncertainty propagates so that the corresponding uncertainty on the temperature amounts to ∼9 mK (this latter being a type B component). Other minor contributions (of the type B) arise from the uncertainty on the Gaussian and Lorentzian components of the UV radiation width (<1 mK), as well as the natural width of the line (∼3 mK).

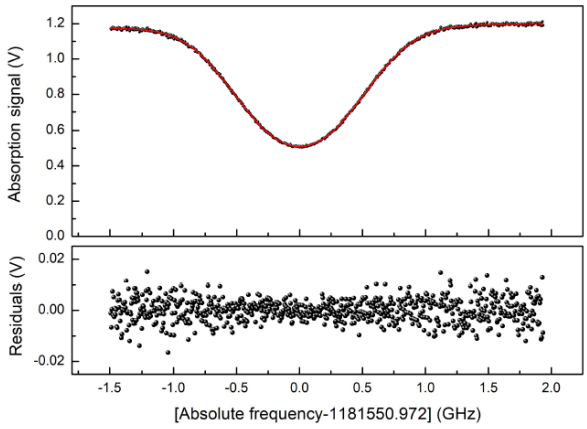

FIG. 9. Example of comb-calibrated absorption spectrum at a cell's temperature of 268.14997 (5) K, as measured by means of the capsule-type standard platinum resistance thermometer. This latter corresponds to a Hg vapor pressure of 16 mPa. The spectrum is obtained after averaging over four spectral acquisitions. The theoretical profile is also shown (red solid line), along with the fit residuals (lower panel). The SNR amounts to ∼300.

VI. CONCLUSIONS

We developed a frequency chain that links the deep UV region to a near-infrared optical frequency comb synthesizer, in order to perform temperature metrology by means of precision spectroscopy of the mercury intercombination line at 253.7 nm. The coherence proper- ties of the comb-locked pump laser were carefully investigated by direct comparison with an ultra-narrow linewidth laser source at 1542 nm, using the technique of direct optical digital synthesis. So doing, it was possible to estimate the spectral width of the UV laser radiation, also reconstructing the line emission profile. This latter was properly considered in the refined analysis of the experimental spectra, for the aims of an accurate quantification of the Doppler broadening effect. Currently, the correction resulting from the UV radiation profile is a factor of 10 smaller than the statistical uncertainty on the spectroscopic temperature. It will be significant once the measurement precision will be increased. In any case, as a result of the present study, it turns out that the contribution of the UV radiation width to the uncertainty budget is negligible at the accuracy level of 1 mK. The first spectroscopic measurement of the thermodynamic temperature of mercury vapors is in good agreement with the c-SPRT's value and exhibits an uncertainty that is largely dominated by the statistical component (∼780 ppm). To approach the target accuracy of 1 mK, it will be necessary to improve significantly the signal-to-noise ratio of the Doppler-broadened spectra, which is the current limiting factor. This is feasible by doing spectral averaging over long times, a viable solution that in principle can be implemented thanks to the frequency stability of the comb-locked spectrometer. Obviously, the averaging time shall be carefully quantified through a dedicated study aimed at finding the trade-off between increasing the signal-to-noise ratio and preserving the spectral fidelity. Moreover, a better detector with a lower noise equivalent power should be used. In this regard, we plan to replace the SiC detector with a nanostructured silicon photodiode with self-induced junction, for which an ex- ternal quantum efficiency above 130% without external amplification has been recently demonstrated, in the UV range [35]. Finally, we plan to further investigate the influence of the collisional effects by doing Doppler-limited measurements in a relatively wide temperature interval, namely, from -30 up to 30 °C. This is necessary to con- firm the pressure broadening parameter resulting from sub-Doppler measurements, which has been adopted in the present work, and to reduce the uncertainty associated to the collisional width.

ACKNOWLEDGMENTS

This research was funded by the Italian Ministry for University and Research (Program Type PRIN 2015).

REFERENCES

[1] L. Gianfrani, Philosophical Transactions of the Royal Society A: Mathematical, Physical and Engineering Sciences **374**, 20150047 (2016).
[2] R. Holzwarth, M. Zimmermann, T. Udem, and T. Hänsch, IEEE Journal of Quantum Electronics **37**, 1493 (2001).
[3] A. Shelkovnikov, R. J. Butcher, C. Chardonnet, and A. Amy-Klein, Phys. Rev. Lett **100**, 150801 (2008).
[4] T. Rosenband, D. B. Hume, P. O. Schmidt, C. W. Chou, A. Brusch, L. Lorini, W. H. Oskay, R. E. Drullinger, T. M. Fortier, J. E. Stalnaker, S. A. Diddams, W. C. Swann, N. R. Newbury, W. M. Itano, D. J. Wineland, and J. C. Bergquist, Science **319**, 1808 (2008).
[5] F. M. Cozijn, P. Dupré, E. J. Salumbides, K. Eikema, and W. Ubachs, Phys. Rev. Lett. **120**, 153002 (2018).
[6] A. Beyer, L. Maisenbacher, A. Matveev, R. Pohl, K. Khabarova, A. Grinin, T. Lamour, D. C. Yost, T. W. Hänsch, N. Kolachevsky, and T. Udem, Science **358**, 79 (2017).
[7] E. Oelker, R. Hutson, C. Kennedy, L. Sonderhouse, T. Bothwell, A. Goban, D. Kedar, C. Sanner, J. Robinson, G. Marti, *et al.*, Nature Photonics **13**, 714 (2019).
[8] I. Pupeza, C. Zhang, M. Högner, and J. Ye, Nature Photonics **15**, 175 (2021).
[9] A. Ozawa, J. Rauschenberger, C. Gohle, M. Herrmann, D.R. Walker, V. Pervak, A. Fernandez, R. Graf, A. Apolonski, R. Holzwarth, F. Krausz, T. W. Hänsch, and T. Udem, Phys. Rev. Lett. **100**, 253901 (2008).
[10] H. R. Telle, B. Lipphardt, and J. Stenger, Applied Physics B **74**, 1 (2002).
[11] I. Galli, F. Cappelli, P. Cancio, G. Giusfredi, D. Mazzotti, S. Bartalini, and P. De Natale, Optics Express **21**, 28877 (2013).
[12] G. Di Domenico, S. Schilt, and P. Thomann, Applied optics **49**, 4801 (2010).
[13] N. Bucalovic, V. Dolgovskiy, C. Schori, P. Thomann, G. Di Domenico, and S. Schilt, Applied optics **51**, 4582 (2012).
[14] D. Elliott, R. Roy, and S. Smith, Physical Review A **26**, 12 (1982).
[15] H. Dinesan, E. Fasci, A. d'Addio, A. Castrillo, and L. Gianfrani, Optics Express **23**, 1757 (2015).
[16] M. Witkowski, G. Kowzan, R. Munoz-Rodriguez,R. Ciuryło, P. S. Żuchowski, P. Masłowski, and M. Zawada, Optics Express **27**, 11069 (2019).
[17] A. Linek, P. Morzyński, and M. Witkowski, Optics Express **30**, 44103 (2022).
[18] S. Mejri, P. L. T. Sow, O. Kozlova, C. Ayari, S. K. Toku- naga, C. Chardonnet, S. Briaudeau, B. Darquié, F. Rohart, and C. Daussy, Metrologia **52**, S314 (2015).
[19] R. Gotti, L. Moretti, D. Gatti, A. Castrillo, G. Galzerano, P. Laporta, L. Gianfrani, and M. Marangoni, Phys. Rev. A **97**, 012512 (2018).
[20] A. Castrillo, E. Fasci, H. Dinesan, S. Gravina, L. Moretti, and L. Gianfrani, Phys. Rev. Appl. **11**, 064060 (2019).
[21] G.-W. Truong, E. F. May, T. M. Stace, and A. N. Luiten, Physical Review A **83**, 033805 (2011).
[22] G.-W. Truong, J. Anstie, E. May, T. Stace and A. Luiten, Nature communications **6**, 1 (2015).
[23] G.-W. Truong, J. D. Anstie, E. F. May, T. M. Stace, and A. N. Luiten, Phys. Rev. A **86**, 030501 (2012).
[24] G.-W. Truong, D. Stuart, J. D. Anstie, E. F. May, T. M. Stace, and A. N. Luiten, Metrologia **52**, S324 (2015).
[25] C. Clivati, S. Gravina, A. Castrillo, G. A. Costanzo, F. Levi, and L. Gianfrani, Optics Letters **45**, 3693 (2020).
[26] T. Hansch and B. Couillaud, Optics communications **35**, 441 (1980).
[27] G. Lopardo, F. Bertiglia, A. Barbone, M. Bertinetti, R. Dematteis, D. Giraudi, and L. Gianfrani, Measurement **173**, 108594 (2021).
[28] G. M. Stéphan, T.T. Tam, S. Blin, P. Besnard, and M. Têtu, Phys. Rev. A **71**, 043809 (2005).
[29] N. R. Newbury and W.C. Swann, JOSA B **24**, 1756 (2007).
[30] F. L. Walls and A. Demarchi, IEEE Transactions on In- strumentation and Measurement **24**, 210 (1975).
[31] M. Delehaye, J. Millo, P.-Y. Bourgeois, L. Groult, R. Boudot, E. Rubiola, E. Bigler, Y. Kersalé, and C. Lacroûte, IEEE Photonics Technology Letters **29**, 1639 (2017).
[32] S. Herbers, S. Dörscher, E. Benkler, and C. Lisdat, Opt. Express **27**, 23262 (2019).
[33] S. Gravina, C. Clivati, A. Castrillo, E. Fasci, N. Chishti, G. Galzerano, F. Levi, and L. Gianfrani, Physical Review Research **4**, 033240 (2022).
[34] S. Gravina, C. Clivati, N. A. Chishti, A. Castrillo, E. Fasci, F. Bertiglia, G. Lopardo, A. Sorgi, N. Coluccelli, G. Galzerano, P. C. Pastor, F. Levi, and L. Gianfrani, Journal of Physics: Conference Series **2439**, 012015 (2023).
[35] M. Garin, J. Heinonen, L. Werner, T. P. Pasanen, V. Vähänissi, A. Haarahiltunen, M. A. Juntunen, and H. Savin, Phys. Rev. Lett. **125**, 117702 (2020).